ELSEVIER

Journal of Organometallic Chemistry 550 (1998) 221–231

Journal of Organometallic Chemistry

Multinuclear NMR studies on substituted derivatives of $Rh_6(CO)_{16}$ in solution [1]

Sergey P. Tunik [a], Ivan S. Podkorytov [b], Brian T. Heaton [c,*], Jonathan A. Iggo [c], Jeyagowry Sampanthar [c]

[a] *St. Petersburg University, Department of Chemistry, Universitetskii pr. 2, St. Petersburg, 198904, Russia*
[b] *S.V. Lebedev Central Synthetic Rubber Research Institute, Gapsalskaya 1, St. Petersburg, 198035, Russia*
[c] *Department of Chemistry, University of Liverpool, P.O. Box 147, Liverpool L69 72D, UK*

Received 13 February 1997

Abstract

Multinuclear NMR data (^{13}C, ^{31}P, ^{13}C–{^{31}P}, ^{13}C–{^{103}Rh} and ^{31}P–{^{103}Rh}) for a series of mono- and di-substituted derivatives of $Rh_6(CO)_{16}$ containing neutral two electron donor ligands [$Rh_6(CO)_{15}L$, (L = NCMe, py, cyclooctene, PPh_3, $P(OPh)_3$,1/2(μ_2,η^1:η^1-dppe)); $Rh_6(CO)_{14}$(LL), (LL = *cis*-CH_2=CMe-CMe=CH_2, dppm, dppe, ($P(OPh)_3)_2$)] are reported; these data show that the solid state structure is maintained in solution. Detailed assignments of the ^{13}CO NMR spectra of $Rh_6(CO)_{15}(PPh_3)$ and $Rh_6(CO)_{14}$(dppm) clusters have been made on the basis ^{13}C–{^{103}Rh} double resonance measurements and the specific stereochemical features of the observed long range couplings in these clusters have been studied. The stereochemical dependence of $^3J(P–C)$ for terminal carbonyl ligands is discussed and the values of $^3J(P–C)$ are found to be mainly dependent on the bond angles in the P–Rh–Rh–C fragment; these data enable the fine structure of the complex multiplets in the ^{13}C–{^1H} and ^{31}P–{^1H} NMR spectra of $Rh_6(CO)_{14}$ (dppm) to be simulated. Variable temperature ^{13}C–{^1H} NMR measurements on $Rh_6(CO)_{15}(PPh_3)$ reveal the carbonyl ligands in this complex to be fluxional. The fluxional process involves exchange of all the CO ligands except the two terminal CO's associated with the rhodium *trans* to the substituted rhodium and can be explained by a simple oscillation of the PPh_3 on the substituted rhodium atom aided by concomitant exchange of the unique terminal CO on this rhodium with adjacent μ_3-CO's. © 1998 Elsevier Science S.A.

Keywords: Multinuclear NMR; $Rh_6(CO)_{16}$; Rhodium

1. Introduction

Multinuclear NMR is a very useful and powerful method for elucidating the structure of organometallic compounds in solution. A great deal of structural information has been obtained using ^{13}C NMR spectroscopy in the study of transition metal carbonyl clusters, see for example Refs. [1–6] and the references therein, including the structural characterization of reactive catalytic species [7]. The presence of other magnetic nuclei in transition metal carbonyl clusters (TMCC's) (e.g., ^1H, ^{31}P, ^{103}Rh, ^{195}Pt) is particularly useful since the multiplicity of the NMR resonances and the dependence of the spin–spin coupling constants (SSCC) allows the structure and fluxional processes of clusters to be elucidated in solution. Direct decoupling techniques {^{31}P, ^{103}Rh} together with PANIC simulation of the observed resonances can be used successfully in such structural studies. The latter approach does not require complex hardware, as for example in the case of ^{13}C–{^{103}Rh} measurements, but requires a good experimental database in order to provide the necessary insight into the variations of spin–spin coupling constants with systematic changes in stereochemistry in quite complicated molecules. In the present paper, we report high resolution multinuclear NMR studies of substituted derivatives $Rh_6(CO)_{16}$ with various two-electron donor ligands: NCMe, py, cyclooctene, dimethylbutadiene, PPh_3, $P(OPh)_3$, dppm, dppe. Variable temperature NMR measurements allow the molecular structure of the clusters in solution to be established together with a detailed understanding of the mechanism of CO-migration in $Rh_6(CO)_{15}(PPh_3)$. The effect on the magnitude of the

* Corresponding author.

[1] This paper is dedicated to Professor Ken Wade on his retirement for his outstanding contributions to chemistry and particularly to enabling a better understanding of cluster chemistry.

long range SSCC's of variations in the relative stereochemistry of P-donor and CO ligands in substituted derivatives of $Rh_6(CO)_{16}$ is also analysed.

2. Results and discussion

2.1. $Rh_6(CO)_{16}$ substituted derivatives with nonphosphorus ligands

2.1.1. Monosubstituted $Rh_6(CO)_{15}L$ clusters (L = NCMe (I), py (II), cyclooctene (III))

Replacement of one CO in $Rh_6(CO)_{16}$ by non-phosphorus-containing ligands can occur with an ionic ligand or a neutral 2-electron donor ligand. Previously reported examples of $[Rh_6(CO_{15}L]^{n-}$ include ($n = 1$, L = H [8], Cl, Br, I, CN, SCN, OCN, COOR, CONHR [9]; $n = 0$, L = NCMe (I), py (II) [10], 4-vinylpyridine [11], cyclooctene (III) [12], SMe_2 [13]). X-ray crystal structure determinations of $[Rh_6(CO)_{15}L]^{n-}$ ($n = 1$, L = Cl [14], I [15], COEt [16], COOMe [16]; $n = 0$, L = SMe_2 [13], 4-vinylpyridine [11]) show that all these derivatives have similar structures; the ligand, L, substitutes one of the twelve terminal CO's in the parent cluster with the general disposition of the other CO's remaining unchanged. This structure is shown schematically in Fig. 1 and has idealized C_s symmetry. There is a plane of symmetry passing through Rh(A), Rh(D) and the centres of the Rh(B)–Rh(B′) and Rh(C)–Rh(C′) vectors. The expected number of ^{13}CO resonances for this structure, has been discussed earlier [6,8] and confirmed in solution by ^{13}C, ^{103}Rh and ^{13}C–{^{103}Rh} NMR studies of the anionic clusters, $[Rh_6(CO)_{15}X]^-$ (X = H, I, CN, SCN). The ^{13}CO spectra of these clusters show three low field multiplets in the ratio 2:1:1 due to the μ_3-CO's and these usually appear as distorted quartets because the coupling to the different rhodiums is almost the same; the eleven terminal CO's appear as doublets with relative intensities 2:2:2:2:2:1. The spectra of the monosubstituted clusters (I–III) (see Table 1 and Fig. 2) have not been assigned in detail but are in complete agreement with this predicted pattern. An accidental overlap of two doublets in the spectrum of (I) (Fig. 2b) can be resolved by changing the solvent (see Fig. 2a) or by varying the temperature. The noncarbonyl ^{13}C NMR resonances in the spectra of (I) and (II) are entirely in accord with N-coordination of both ligands.

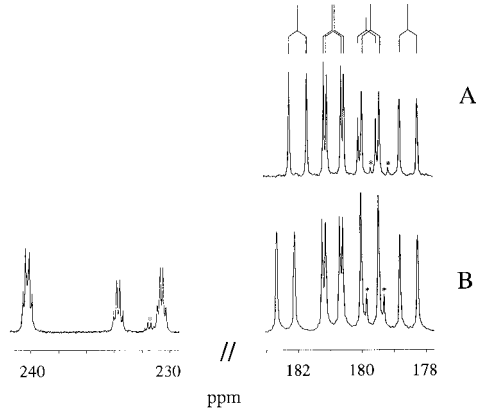

Fig. 2. 125 MHz ^{13}C–{^1H} NMR spectra of $Rh_6(CO)_{15}(NCMe)$ at 297 K. (a) Solvent = $CDCl_3$ / $PhCD_3$ / NCMe = 4/6/1. The terminal CO region only is shown together with a schematic representation of the splitting pattern of the terminal CO ligands. (b) Solvent = $CDCl_3$ / NCMe = 10/1. The resonances marked with asterisks correspond to $Rh_6(CO)_{16}$ present as an impurity.

2.1.2. $Rh_6(CO)_{14}(\eta^4$-s-cis-$CH_2 = CMe–CMe = CH2)$ (IV)

The solid state structure of the disubstituted cluster $Rh_6(CO)_{14}$(dimethylbutadiene) (IV) has been established [17]; the diene ligand replaces two terminal CO's on the same Rh atom and adopts a symmetrical (η^4-*s-cis*) coordination (see Fig. 3). The ^{13}C NMR spectrum of (IV), (Fig. 4 and Table 2), is entirely consistent with this structure being maintained in solution. The two CO ligands on the Rh *trans* to the substituted Rh are *inequivalent*. The possibility of reorientation of the

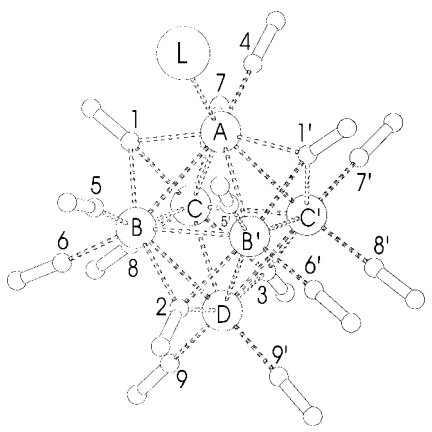

Fig. 1. Schematic representation of the structure of $Rh_6(CO)_{15}L$.

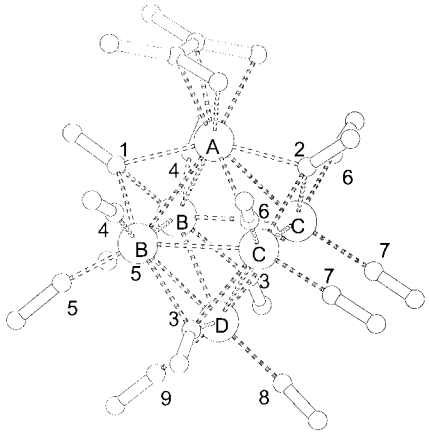

Fig. 3. Schematic representation of the structure of $Rh_6(CO)_{14}(\eta^4$-*cis*-CH_2=CMe–CMe=CH_2).

Table 1
C-13 NMR spectroscopic data for nonphosphorus ligand substituted derivatives of $Rh_6(CO)_{16}$ (See Fig. 1 for numbering scheme)

Cluster			μ_3-CO				δ(CO)[a]	Terminal CO				Other resonances	Assign-ments
	Solvent	T K	C(1)O	C(2)O	C(3)O	C(4)O	C(5)O	C(6)O	C(7)O	C(8)O	C(9)O		
$Rh_6(CO)_{15}$(NCMe) (I)	b	297	244.2 (30.5, 33.8)	233.7[c] (27.7)	230.6[c] (25.9)	179.8 (69.2)	182.8[d] (70.0)	181.3[d] (68.4)	181.2[d] (67.9)	179.7[d] (68.6)	178.6[d] (69.5)	123.9	MeCN
$Rh_6(CO)_{15}$(py) (II)	e	320	246.4 (22.7, 34.7)	233.2[c] (28.5)	230.9[c] (27.0)	181.3 (69.9)	182.5[d] (70.3)	181.0[d] (66.5)	180.7[d] (68.6)	181.4[d] (68.5)	179.2[d] (68.7)	153.3 138.4 126.0	py
$Rh_6(CO)_{15}$(cyclooctene) (III)	f	297	237.4 (27.4)	233.1[c] (27.7)	231.6[c] (27.5)	180.9 (71.4)	183.1[d] (70.4)	181.1[d] (69.0)	180.5[e] (65.2)	180.1[d] (68.1)			

[a]Figures in parentheses are ^{1}J(Rh-CO); [b]$PhCD_3$:$CDCl_3$:MeCN = 6:4:1; [c]Assignments could be interchanged, relative intensity 1; [d]Assignments not made, all of relative intensity 2; [e]$CDCl_3$; [f]$CDCl_3$: cyclooctene = 95:5.

Table 2
C-13 NMR spectroscopic data for $Rh_6(CO)_{14}(\eta^4$-cis-CH_2=CMe-CMe=CH_2) (IV) in $CDCl_3$ at 297 K (see Fig. 3 for numbering scheme)

Cluster	μ3-CO			δ(CO)[a]		Terminal CO				
	C(1)O	C(2)O	C(3)O	C(4)O	C(5)O	C(6)O	C(7)O	C(8)O	C(9)O	
$Rh_6(CO)_{15}$(dimethylbutadiene) (IV)	244.5[b] (27.6)	239.9[b] (26.4)	232.9 (26.4)	183.7[c] (70.0)	183.5[c] (69.9)	181.7[c] (67.0)	180.7[c] (66.9)	180.6[d] (67.9)	180.1[d] (70.0)	

[a]Figures in parentheses are ^{1}J(Rh-CO); [b]Assignments could be interchanged, relative intensity 1; [c]Assignments not made, all of relative intensity 2; [d]Assignments could be interchanged, relative intensity 1.

Table 3
Spectroscopic data for P-donor substituted derivatives of the type $Rh_6(CO)_{15}L$ (For numbering scheme, see Fig. 1)

	$Rh_6(CO)_{15}(PPh_3)$ (V)[a]			$Rh_6(CO)_{15}\{P(OPh)_3\}$ (VI)[b]			$[\{Rh_6(CO)_{15}\}_2(\mu_2,\eta^1{:}\eta^1\text{-dppe})]$ (VII)[b]		
Assignment	δ(X)	^{1}J(Rh-CO)	Other SSCC's	δ(X)	^{1}J(Rh-CO)	Other SSCC's	δ(X)	^{1}J(Rh-CO)	Other SSCC's
C(1)O	239.6	19, 19, 20.0		236.8	25.8		239.4	26.1	
C(2)O	236.7	27.4		235.0[g]	26.6		236.2[g]	27.6	
C(3)O	232.1	28.1		231.6[g]	27.5		232.2[g]	27.9	
C(4)O	183.5	69.5	d	180.9	68.5	i	182.95	70	l
C(5)O	182.0	70.2		181.9[h]	70.0		183.0[h]	69.3	
C(6)O	180.1	65.8		180.6[h]	66.4		182.3[h]	69.8	
C(7)O	182.7	69.7		182.0[h]	69.5		180.0[h]	66.4	
C(8)O	182.1	69.7	e	181.8	68.7	j	182.0	69.7	m
C(9)O	179.4	68.7		180.3[h]	68.3		179.4[h]	68.6	
P	25.4		f	106.3		k	23.3		n
Rh(A)	-303[c]								
Rh(B)	-445[c]								
Rh(C)	-347[c]								
Rh(D)	-484[c]								

[a] In $CDCl_3$ at 250 K; [b] In $CDCl_3$ at 297 K; [c] Rh NMR data obtained in $CDCl_3$ at 213 K from ^{13}C-{^{103}Rh} measurements; [d] ^{2}J(P-CO) 13.3 Hz; [e] ^{3}J(P-CO) 20.7 Hz; [f] ^{1}J(Rh-P) 134.6 Hz; [g] Assignments not made, all resonances of relative intensity 1; [h] Assignments not made, all resonances of relative intensity 2; [i] ^{2}J(P-CO) 10.3 Hz; [j] ^{3}J(P-CO) 36.3 Hz; [k] ^{1}J(Rh-P) 240.0, ^{2}J(Rh-P) 8.6 Hz; [l] ^{2}J(P-CO) 10.0 Hz; [m] ^{2}J(P-CO) 20.0 Hz; [n] ^{1}J(Rh-P) 135.5 Hz.

dimethylbutadiene on the substituted Rh can be eliminated since this would lead to fewer than the observed number of resonances.

Although ^{13}C–{^{103}Rh} NMR measurements on (IV) have not been made to enable a detailed assignment of the μ_3-CO's or the terminal CO's, nevertheless, the presence of two resonances of relative intensity 1 due to C(8)O and C(9)O (Fig. 3 and 4 and Table 2) unambiguously means that dimethylbutadiene is static on Rh(A) at room temperature.

2.1.3. Monosubstituted derivatives of $Rh_6(CO)_{16}$, $Rh_6(CO)_{15}L$ ($L = PPh_3$ (V), $P(OPh)_3$) (VI)) and $[\{Rh_6(CO)_{15}\}_2(\mu_2,\eta^1{:}\eta^1\text{-dppe})]$ (VII))

The present work, (Table 3) describes NMR studies on $Rh_6(CO)_{16}L$ ($L = PPh_3$ (V), $P(OPh)_3$ (VI)), and $[\{Rh_6(CO)_{15}\}_2(\mu_2,\eta^1{:}\eta^1\text{-}Ph_2PCH_2CH_2PPh_2)]$ (VII). The solid state structures of (V) [18] and (VI) [19] are strictly related to all the other monosubstituted clusters and the schematic representation shown in Fig. 1 will be used to discuss the relationship between the observed spectroscopic parameters and the stereochemistry of the monosubstituted clusters.

$L = PPh_3$ (V).

Variable temperature ^{13}C–{^{1}H} NMR spectra of (V) have already been reported [22] but no carbonyl assignments were made. Above 213 K, (V) exhibits carbonyl fluxionality and we now describe low temperature measurements which allow unambiguous assignments of both the ^{13}CO and ^{103}Rh resonances, so that the mechanism of the fluxional process, can be understood in detail.

The 125 MHz ^{13}C–{^{1}H} NMR spectrum of (V) in $CDCl_3$ at 213 K is shown in Fig. 5 and the NMR data are summarised in Table 3. As expected for the static structure, there are three sets of resonances due to four face-bridging carbonyls in the ratio of 2:1:1 due to C(1)O, C(2)O and C(3)O, respectively, and six sets of

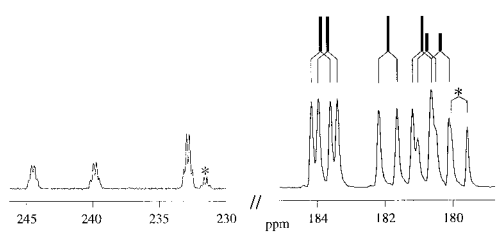

Fig. 4. 125 MHz ^{13}C–{^{1}H} NMR spectrum of $Rh_6(CO)_{14}$(dimethylbutadiene) in $CDCl_3$ at 297 K together with a schematic representation of the splitting pattern of the terminal CO ligands. The resonances marked with asterisks correspond to $Rh_6(CO)_{16}$ present as an impurity.

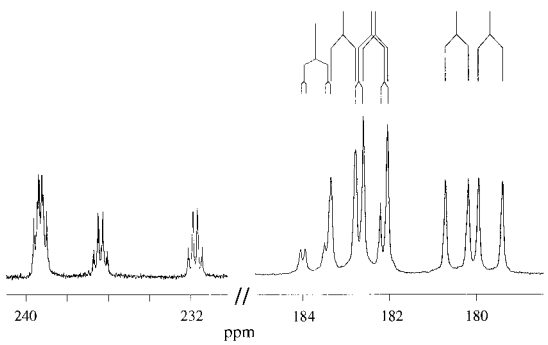

Fig. 5. 125 MHz ^{13}C–{^{1}H} NMR spectrum of $Rh_6(CO)_{15}(PPh_3)$ in $CDCl_3$ at 215 K and a schematic representation of the splitting pattern of the terminal CO ligands.

Table 4
Bond angles, dihedral angles and the *cis/trans* disposition of the P-Rh-Rh-CO fragment about the Rh-Rh bond in $Rh_6(CO)_{15}(PPh_3)$

Atoms	P-Rh-Rh bond angles (°)	Rh-Rh-C bond angles (°)	dihedral angles (°)	*cis/trans* disposition (Pn)
P-Rh(A)-Rh(B)-C(5)	111.8	102.8	7	*cis-cis* (**P1**)
P-Rh(A)-Rh(B)-C(5′)	110.8	104.8	14	*cis-cis* (**P1**)
P-Rh(A)-Rh(B)-C(6)	111.8	145.5	94	*cis-trans* (**P2**)
P-Rh(A)-Rh(B)-C(6′)	110.8	140.8	101	*cis-trans* (**P2**)
P-Rh(A)-Rh(C)-C(7)	150.7	97.8	73	*trans-cis* (**P3**)
P-Rh(A)-Rh(C)-C(7′)	149.5	97.1	80	*trans-cis* (**P3**)
P-Rh(A)-Rh(C)-C(8)	150.7	145.6	27	*trans-trans* (**P4**)
P-Rh(A)-Rh(C)-C(8′)	149.5	148.7	33	*trans-trans* (**P4**)

terminal carbonyl resonances in the ratio of 1:2:2:2:2:2 (C(4)O–C(9)O). In addition to $1J$(Rh–C), long range couplings ^nJ(P–C) ($n = 2$ and 3) are found for some terminal carbonyls. There is presently a lack of experimental data long-range coupling constants in transition metal carbonyl clusters and one of the aims of this research was to test the applicability of empirical correlations that have been found to be valid for other compounds for the assignment of such long range couplings. In the case of three bond couplings, two geometrical factors affecting the magnitude of ^3J(P–C) in a fragment P–Rh(X)–Rh(Y)–C(Z) need to be considered:

(i) The bond angles P–Rh(X)–Rh(Y) and Rh(X)–Rh(Y)–C(Z). It is well known that two bond couplings are greater for trans than for *cis*-dispositions of interacting nuclei [20]. Extension of this idea to the fragment P–Rh(X)–Rh(Y)–C(Z) in the clusters under consideration leads to the expectation that the two bond angles (P–Rh–Rh and Rh–Rh–C) should have a marked effect on the value of ^{3}J(P–C) with *trans–trans* > *trans–cis* ≈ *cis–trans* > *cis–cis*; the crystallographically determined angles for $Rh_6(CO)_{15}(PPh_3)$ are given in Table 5.

(ii) The dihedral angle ϕ between the planes P–Rh(X)–Rh(Y) and Rh(X)–Rh(Y)–C. In many compounds the magnitude of ^3J can be related to the dihedral angle following the Karplus equation [21], which predicts a minimum value of ^{3}J when $\phi = 90°$ and a maximum value of ^{3}J when $\phi = 0°$ or 180°.

It can be supposed that the magnitude of ^{3}J is controlled by each of these two factors. Thus, ^{3}J(P–C) is expected to reach a maximum when there is a *trans–trans* configuration with ϕ close to 0° or 180°. Conversely, ^{3}J(P–C) will be at a minimum when there is a cis–cis configuration with ϕ close to 90°. For the clusters under study, including $Rh_6(CO)_{15}(PPh_3)$, there are four configurations of the P–Rh(X)–Rh(Y)–C(Z) fragment, which are described below and in Table 4.

Table 5
Spectroscopic data for P-donor substituted derivatives of the type $Rh_6(CO)_{14}(LL)$ (LL = $(P(OPh)_3)_2$; dppm; dppe) (For numbering scheme, see Figs. 10 and 12)

	trans-$Rh_6(CO)_{14}\{P(OPh)_3\}_2$ (VIII)[a]			$Rh_6(CO)_{14}(\mu_2$-dppm) (IX)[b]			$Rh_6(CO)_{14}(\mu_2$-dppe) (X)[b]		
Assignment	δ(X)	^{1}J(Rh-CO)	Other SSCC's	δ(X)	^{1}J(Rh-CO)	Other SSCC's	δ(X)	^{1}J(Rh-CO)	Other SSCC's
C(1)O	238.5[c1]	21.4, 28.5, 30.5		249.7	26.2		252.6[c1]	30	
C(2)O	235.0[c1]	22.8, 29.2		240.1	26.0		239.4	24.0	
C(3)O	181.05	69.0	d	232.2	28.2		232.2[c1]	28.0	
C(4)O	182.6[c2]	69.3		185.5[c]	70.7		186.2[c2]	70.6	
C(5)O	183.8[c3]	69.4	e	181.1[c]	65.4		180.2[c2]	64.8	
C(6)O	183.6[c3]	69.0	f	184.4	68.1[h]	i	185.1	68.0	l
C(7)O	182.5[c2]	67.0		183.1	68.1	j	184.3[c3]	69.9	m
C(8)O				183.3	70.1		182.9	69.3	
C(9)O				181.7	69.6	k	182.5[c3]	64.4	n
P	106.5		g	11.6		l	18.6		o
Rh(A)				-432[p]					
Rh(B)				-306[p]					
Rh(C)				-332[p]					
Rh(D)				-276[p]					

[a] In $CDCl_3/C_6H_5CD_3$ at 297 K; [b] In $CDCl_3$ at 297 K; [c] Assignments could be interchanged with corresponding superscript; [d] ^{2}J(P-CO) 10.8 Hz; [e] ^{3}J(P-CO) 35.4 Hz; [f] ^{3}J(P-CO) 37.8 Hz; [g] ^{1}J(Rh-P) 241.0, ^{2}J(Rh-P) 8.0 Hz; [h] See Fig. 14 for values of other SSCC's; [i] ^{2}J(P-CO) 7 Hz; [j] ^{3}J(P-CO) 21.7 Hz; [k] ^{3}J(P-CO) 22.7 Hz; [k] ^{1}J(Rh-P) 141.6, ^{2}J(P-P′) 47.5 Hz; [l] ^{2}J(P-CO) 9.9 Hz; [m] ^{3}J(P-CO) 19.4 Hz; [n] ^{3}J(P-CO) 20.7 Hz; [o] ^{1}J(Rh-P) 140.1 Hz; [p] Rh NMR data obtained in $CDCl_3$ at 297 from ^{13}C-{^{103}Rh} measurements.

cis–cis with $\phi \approx 0°$ (C(5) and C(5′)) **P1**
cis–trans with $\phi \approx 90°$ (C(6) and C(6′)) **P2**
trans–cis with $\phi \approx 90°$ (C(7) and C(7′)) **P3**
trans–trans with $\phi \approx 0°$ (C(8) and C(8′)) **P4**

For the **P1–P3** configurations, factors (i) and (ii) act in opposite directions resulting in intermediate or small values of ^{3}J(P–C). In the **P4** configuration, the geometric effects reinforce each other and would be expected to result in a maximum value of ^{3}J(P–C).

Assignment of only two terminal carbonyl resonances in the ^{13}C–{^{1}H} NMR spectrum of (V) can be made easily on the basis of either the relative intensity and/or long range P–C coupling; *viz* the doublet of doublets at 183.5 with relative intensity 1 can be assigned unambiguously to C(4)O arising from both ^{1}J(Rh–C) and ^{2}J(P–C). Of all the other terminal carbonyl resonances of relative intensity 2, only the resonance at 182.1 ppm shows additional P–C coupling. From the above discussion, this corresponds to the unique configuration **P4** and allows the unambiguous assignment of this resonance to C(8)O and C(8′)O. This is an important conclusion, which is further substantiated by direct ^{13}C–{^{103}Rh} measurements and also allows Rh(B) to be distinguished from Rh(C).

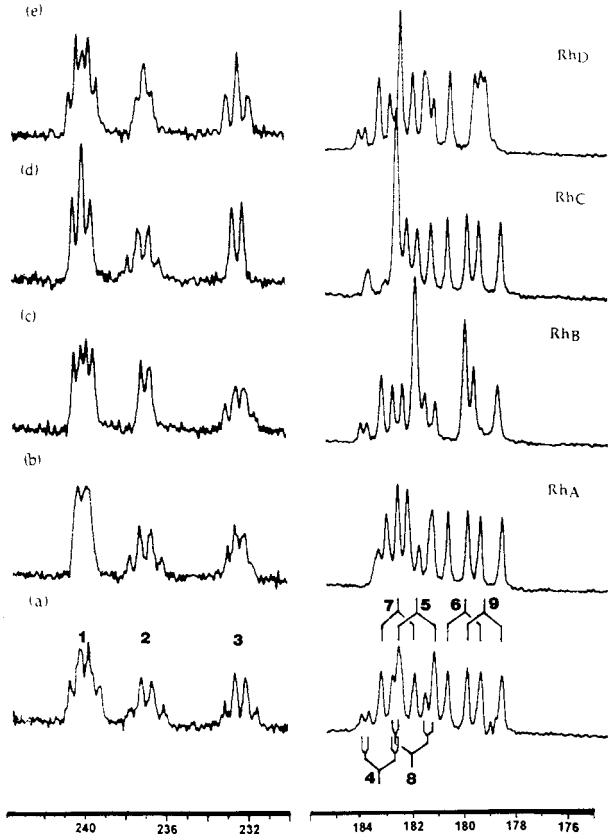

Fig. 6. ^{13}C–{^{103}Rh} NMR spectra (50.3 MHz) of $Rh_6(CO)_{15}(PPh_3)$ in $CDCl_3$ at 213 K: (a) fully coupled, (b) Rh(A) decoupled (c), Rh(B) decoupled, (d) Rh(C) decoupled, and (e) Rh(D) decoupled.

Assignment of the remaining ^{13}C resonances of (V) has been made on the basis of ^{13}C–{^{103}Rh} measurements (see Fig. 6). These measurements, in combination with the coupling model proposed above allow straightforward and unambiguous assignment of the ^{13}CO resonances, which are summarised in Table 3. The ^{31}P–{^{1}H} NMR spectrum of (V) shows a doublet at 25.4 ppm with ^{1}J(Rh–P) 134.6 Hz. ^{31}P–{^{103}Rh} NMR measurements confirm the Rh(A) frequency found from the ^{13}C–{^{103}Rh} NMR measurements.

Further confirmation of the assignments of the resonances due to the terminal carbonyls on Rh(A) and Rh(C) is obtained from ^{13}C–{^{31}P} NMR measurements. Thus, on irradiation of the phosphorus the doublet of doublets at 183.5 and 182.1 ppm collapse to doublets (due to residual coupling with Rh(A) and Rh(C), respectively).

In contrast to the parent cluster $Rh_6(CO)_{16}$ which shows no carbonyl scrambling below $+70°C$, $Rh_6(CO)_{15}(PPh_3)$ is fluxional. Having assigned the limiting low temperature spectra, it is clear from the previously published variable temperature ^{13}C NMR spectra that all the CO's are involved in exchange *except for C(9)O*. A mechanism consistent with the observed variable temperature spectra is shown in Fig. 7; essentially PPh_3 oscillates about Rh_A. This exchange mechanism has been confirmed by 2D NOESY measurements. Crosspeaks linking the following CO ligands are observed: C(1)O ↔ C(4)O, C(2)O ↔ C(3)O, C(5)O ↔ C(7)O, C(6)O ↔ C(8)O and C(9)O does not take part in the exchange.

The proposed mechanism occurs as a result of concomitant oscillation of PPh_3 from being over the Rh(A)Rh(B)Rh(B′)-face to being over the Rh(A)Rh(C)Rh(C′)-face and interconversion of C(1) with C(4)O and C(4′)O as shown in Fig. 7. This concerted movement only involves PPh_3, C(1)O, C(4)O and C(4′)O which results in the ''symmetry'' transformation of the other pairs of carbonyls (2 ↔ 3; 5 ↔ 7; 6 ↔ 8). The fact that C(9)O and C(9)O are not involved in the fluxional process is due to their unique symmetry and is entirely consistent with the mechanism proposed.

L = $P(OPh)_3$ (VI), ($\mu_2,\eta^1:\eta^1 - Ph_2PCH_2CH_2PPh_2$) (VII).

The other two monosubstituted clusters, (VI) and (VII), are stereochemically rigid at room temperature and the general features of the ^{13}C NMR spectra correspond closely with those of (V). The observed spectroscopic parameters are summarised in Table 3 and the ^{13}C NMR spectra of (VI), recorded at two different operating frequencies (50 and 125 MHz), are shown in Fig. 8. Fig. 8b clearly shows that the two doublets at ca. 181.5 ppm, erroneously assigned in previous work [22] to two inequivalent CO ligands, is actually a doublet of doublets centered at 181.8 ppm corresponding to C(8)O,

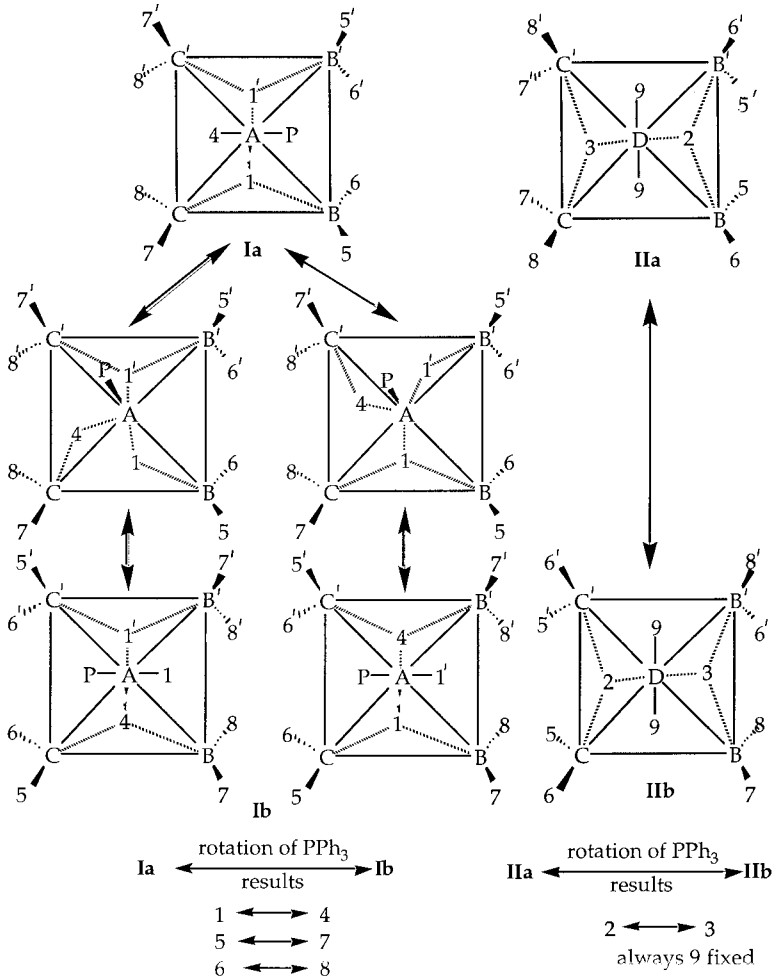

Fig. 7. Schematic representation of the mechanism of ligand exchange in $Rh_6(CO)_{15}(PPh_3)$; I shows a top view the octahedron and II views the octahedron from below. (See Fig. 1 for numbering scheme.)

vide supra (Fig. 1). It is worthwhile mentioning one principal spectroscopic difference between (V) and (VI). The ^{31}P spectrum of (VI) consists of a doublet of triplets as compared to a simple doublet for (V); the additional triplet (8.6 Hz) must arise from $^{2}J(Rh(C)–P)$ since only Rh(C) is *trans* to phosphorus and it is well known that coupling to phosphites is much larger than to phosphines.

The solid state structure of (VII) has previously been determined [18] and shown to consist of two $\{Rh_6(CO)_{15}\}$-fragments with a bridging diphosphine ligand. The $^{13}C–\{^{1}H\}$ NMR spectrum of (VII) is entirely consistent with this structure being retained in solution and the spectroscopic data (Table 3) are very similar to those found for (V) and (VI).

2.2. Disubstituted derivatives $Rh_6(CO)_{14}(LL)$, (LL = $\{P(OPh)_3\}_2$ (VIII), dppm (IX), dppe (X))

Two types of disubstituted $Rh_6(CO)_{16}$ derivatives are studied in the present paper: $Rh_6(CO)_{14}\{P(OPh)_3\}_2$ (VIII), which contains two triphenylphosphites on *trans*-rhodium atoms and $Rh_6(CO)_{14}(\mu_2,\eta^2$-diphosphine) which contains a μ_2-bridging ligand (dppm (IX), dppe (X)) on *cis*-Rh's within the Rh_6-octahedron. The solid state structure and preliminary spectroscopic data for (VIII) and (X) have been reported previously [18,22] and the solid state structure of (IX) has been determined by X-ray crystallography [19].

$$LL = \{P(OPh)_3\}_2 \text{ (VIII)}.$$

The solid state structure of (VIII) is shown in Fig. 9; the two triphenylphosphite ligands replace terminal CO's on *trans*-Rh's in the Rh_6-octahedron in $Rh_6(CO)_{16}$. The symmetry of (VIII) is C_2 with the C_2-axis passing through Rh(C) and Rh(D). The phosphorus atoms in (VIII) are chemically equivalent and the ^{13}C NMR spectrum (Fig. 10) displays all the first order features (Rh–C, P–C couplings) described above for the monosubstituted (V–VII) clusters. Thus, there are two equally intense lowfield μ_3-CO's and two of the five terminal carbonyl resonances, those centered at 182.6 and 182.5

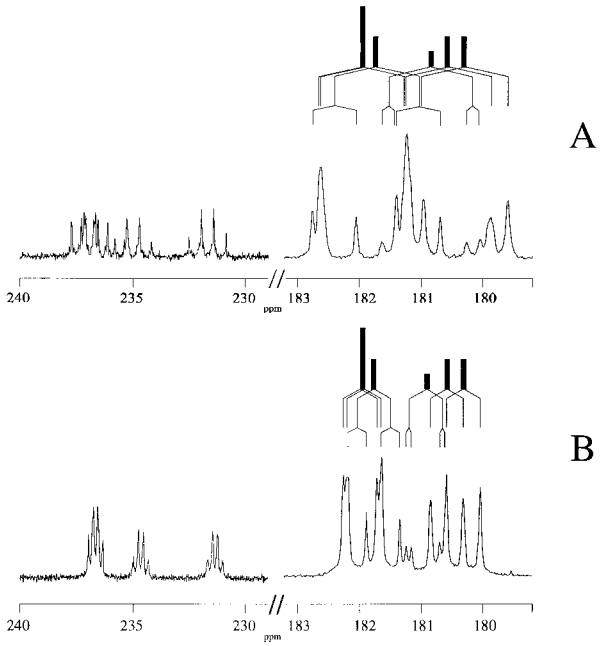

Fig. 8. $^{13}C–\{^1H\}$ NMR spectrum of $Rh_6(CO)_{15}\{P(OPh)_3\}$ in $CDCl_3$ at 297 K recorded at: (a) 50 MHz, and (b) 125 MHz including a schematic representation of the splitting pattern of the terminal CO ligands.

ppm, are simple doublets and can be assigned to C(4)O and C(7)O because of the *trans–cis* disposition of these CO's with respect to the phosphorus atoms of the $P(OPh)_3$ ligands; the three other resonances are doublets of doublets due to two and three bond couplings of the carbonyl carbons C(3), C(5) and C(6) to the phosphorus atoms. The values of ^2J(P–C) and ^3J(P–C) (Table 4) are very close to those found for (VI).

As found for the monosubstituted derivative (VI), the ^{31}P NMR spectrum of (VIII) consists of a simple doublet [^{1}J(Rh–P)] of triplets [^{2}J(Rh–P)] due to the two chemically equivalent phosphorus nuclei.

LL = dppm (IX).

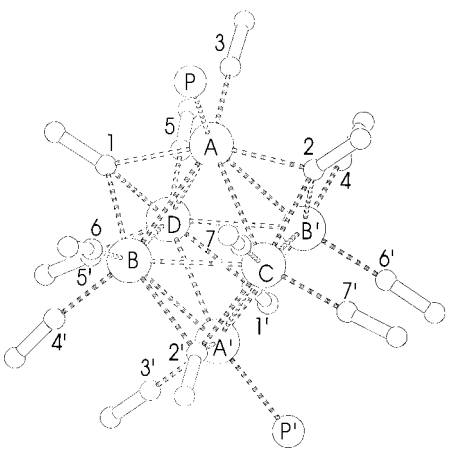

Fig. 9. Schematic representation of the structure of the $Rh_6(CO)_{14}\{P(OPh)_3\}_2$.

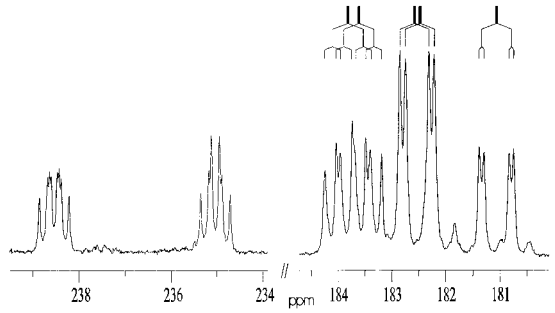

Fig. 10. 125 MHz $^{13}C–\{^1H\}$ NMR spectrum of $Rh_6(CO)_{14}\{P(OPh)_3\}_2$ in $CDCl_3/PhCD_3 = 1/3$ at 297 K and the schematic representation of the splitting pattern of the terminal CO ligands.

The diphosphines (dppm and dppe) are popular ligands for the synthesis of carbonyl cluster derivatives. Both ligands can in principle coordinate to a polynuclear metal core in a bridging or chelating mode. An understanding of the main spectroscopic features associated with each mode of bonding of the diphosphine is of considerable importance for the further application of NMR spectroscopy in the characterization of the structure of polynuclear carbonyls in solution. The solid state structures of $Rh_6(CO)_{14}$(LL) (LL = dppm (IX) dppe (X)) have been established [18,19] and are shown schematically in Fig. 11. The ^{13}C and ^{31}P NMR spectroscopic data are summarised in Table 5.

The observed and simulated $^{31}P–\{^1H\}$ NMR spectra of (IX) (Fig. 12) result from an AA′XX′ spin system arising from the chemically equivalent but magnetically inequivalent P, P′ and Rh(B), Rh(B′) nuclei. $^{31}P–\{^{103}Rh\}$ NMR measurements are also consistent with the proposed description of the spin–spin coupling; thus, decoupling Rh(B) at 7.897570 MHz [$\delta(^{103}Rh(B)) - 306$ ppm] collapses the multiplet to a broad singlet.

Variable temperature $^{13}C–\{^1H\}$ NMR spectra of (IX)

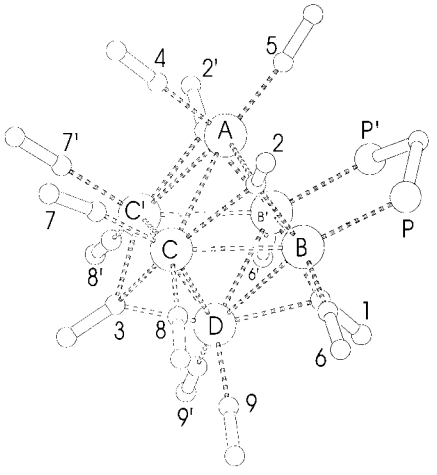

Fig. 11. Schematic representation of the structure of $Rh_6(CO)_{14}(\mu_2, \eta^2$-LL) (LL = dppm, dppe; dppm = $Ph_2PCH_2PPh_2$; dppe = $Ph_2PCH_2CH_2PPh_2$).

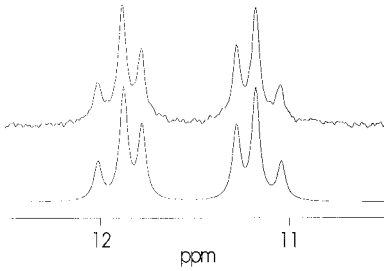

Fig. 12. 202 MHz ^{31}P–{^{1}H} NMR spectrum of $Rh_6(CO)_{14}$(dppm) in $CDCl_3$ at 297 K; top: experimental spectrum, bottom: simulation using AA′XX′ model, AA′ = PP′, XX′ = Rh(B)Rh(B′). See Table 4 for parameters.

in CD_2Cl_2 show that the cluster is stereochemically rigid over the temperature range 297 K to 213 K and the number of carbonyl resonances and their relative intensities are entirely in agreement with the solid state structure. The spectrum in the face-bridging carbonyl region consists of three pseudo quartets of relative intensity 1:2:1 due to C(1)O, C(2)O and C(3)O respectively. The terminal carbonyl region consists of six resonances with intensity ratio of 1:1:2:2:2:2 due to C(4)O, C(5)O, C(6)O, C(7)O, C(8)O and C(9)O, respectively. Some of these resonances are quite complicated due to $^{1}J(^{103}Rh–^{13}C)$ and various long range couplings including ^{2}J(P–C), ^{3}J(P–C) and ^{2}J(P–P).

The selective ^{13}C–{^{103}Rh} NMR spectra of (IX) in CD_2Cl_2 at room temperature allow an almost complete assignment of all the carbonyl resonances. The spectroscopic data (125 MHz, $CDCl_3$; 62.5 MHz, CD_2Cl_2), along with the assignments, are given in Table 5. Although analysis of the spectra is complicated because of spin-tickling when carrying out ^{13}C–{^{103}Rh} measurements on rhodium resonances which are in close proximity, assignment of the ^{103}Rh and ^{13}CO resonances is relatively straightforward. Thus, for example, irradiation at 7.896570 MHz [$\delta(^{103}Rh(A)) - 432$ ppm], causes:

(1) the doublet at 181.8 ppm with relative intensity 1, to collapse to a singlet; therefore this unique terminal carbonyl resonance must be due to either C(4)O or C(5)O; it is impossible to differentiate between these two groups although we favour the resonance at 181.8 ppm being due to C(5)O since this CO is directly above the dppm ligand whereas C(4)O is more similar to the other terminal carbonyls in this structure.

(2) the doublet at 185.5 ppm with relative intensity 1, to collapse to a singlet and this unique resonance is probably due to C(4)O rather than C(5)O, *vide supra*.

(3) the quartet at 240.1 ppm of relative intensity 2, to collapse to a triplet as a result of residual coupling with Rh(B) and Rh(C) and this face-bridging carbonyl resonance must be C(2)O.

As found for (V), the value of ^{3}J(P–C) in (IX) is dependent on the stereochemistry and the bond angles and dihedral angles in the P–Rh(X)–Rh(Y)–C fragments are summarised in Table 6.

The lack of ^{3}J(P–C) for μ_3-CO's is probably due to the longer Rh–CO bond for μ_3-CO's *and/or* the unfavourable disposition of the P and μ_3-CO's which are usually in a *cis*-configuration.

The only other terminal CO resonance which appears as a simple doublet occurs at 183.3 ppm and consideration of the stereochemical factors (Table 4) and ^{13}C–{^{103}Rh} measurements indicate that this is due to C(8)O on Rh(C) as a result of the **P3** environment.

The other multiplets at 184.4, 183.1 and 181.7 ppm are all complicated by long range ^{31}P–^{13}C couplings and have been assigned from ^{13}C–{^{103}Rh} measurements and consideration of Table 4. The resonance at 183.1 ppm is due to C(7)O on Rh(C). This CO ligand occupies a **P4** environment; the resonance has been simulated [23] assuming a six spin system including ^{31}P, ^{31}P′, ^{103}Rh(B), ^{103}Rh(B′), ^{103}Rh(C), and ^{13}C(7) and the coupling parameters obtained from the simulation are given in Fig. 13 and in Table 5.

The resonance at 181.7 ppm can be unambiguously assigned to C(9)O which is also in a **P4** position. The stereochemical environment of C(9)O, at least from the viewpoint of spin coupling, is very similar to C(7)O and a similar six spin model (^{31}P, ^{31}P′, ^{103}Rh(B), ^{103}Rh(B′), ^{103}Rh(D), and ^{13}C(9); see Table 5 for parameters) has been used successfully to simulate this resonance.

The resonance at 184.4 ppm which appears as a

Table 6
Bond and dihedral angles and the *cis/trans* disposition of the P-Rh-Rh-CO fragment about the Rh-Rh bond in [$Rh_6(CO)_{14}$(dppm)]

Atoms	P-Rh-Rh bond angles (°)	Rh-Rh-C bond angles (°)	dihedral angles (°)	*trans/cis* disposition
P-Rh(B)-Rh(A)-C(4)	100.42	144.2	-120.5	*cis-trans* (**P2**)
P′-Rh(B)-Rh(A)-C(4)	99.45	147.7	124.4	*cis-trans* (**P2**)
P-Rh(B)-Rh(A)-C(5)	100.42	105.8	-5.7	*cis-cis* (**P1**)
P′-Rh(B)-Rh(A)-C(5)	99.45	103.1	11.6	*cis-cis* (**P1**)
P-Rh(B)-Rh(C)-C(7)	144.68	145.94	-5.1	*trans-trans* (**P4**)
P′-Rh(B)-Rh(C)-C(7′)O	143.96	146.85	-1.2	*trans-trans* (**P4**)
P-Rh(B)-Rh(C)-C(8)	152.54	96.1	-110.7	*trans-cis* (**P3**)
P′-Rh(B)-Rh(C)-C(8′)	153.81	95.1	108.7	*trans-cis* (**P3**)
P-Rh(B)-Rh(D)-C(9′)	152.54	151.35	-4.1	*trans-trans* (**P4**)
P′-Rh(B)-Rh(D)-C(9)	153.81	147.84	2.5	*trans-trans* (**P4**)

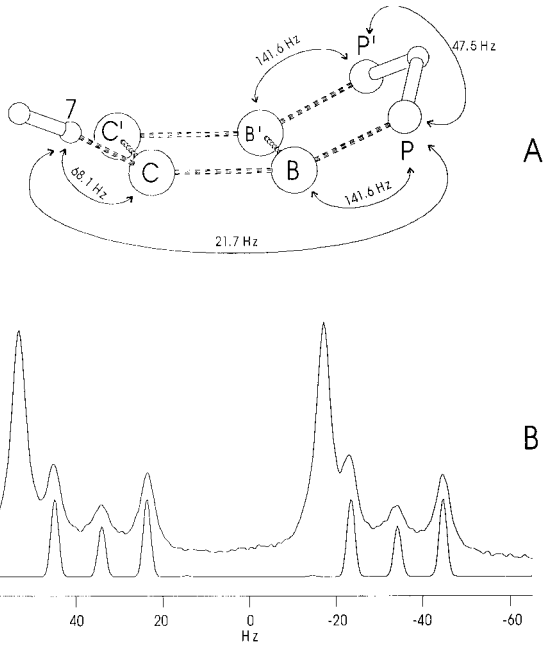

Fig. 13. (A) Schematic representation of the coupling network used in the simulation of the resonance centered at 183.13 ppm (assigned to C(7)) in the ^{13}C NMR spectrum of $Rh_6(CO)_{14}$(dppm). The values of the coupling constants are indicated by arrows. (B) Top: experimental (125 MHz) and bottom: simulated spectrum.

doublet with a shoulder due to ^2J(P–C) ≈ 7 Hz, can be unambiguously assigned to C(6)O in accordance with ^{13}C–{^{103}Rh} data. This simple three spin model (^{13}C(6)–^{103}Rh(B)–^{31}P) is a reasonable initial approximation to describe the experimental spectrum. However, resolution enhancement of this resonance (Fig. 14) reveals further fine structure. In order to simulate this resonance it was necessary to use a six spin system including ^{31}P, ^{31}P′, ^{103}Rh(B), ^{103}Rh(B′), ^{103}Rh(A), and ^{13}C(6) (see Table 5 for parameters). In this model, it is necessary to use a small value for the two bond ^{103}Rh–^{13}C coupling. The inclusion of ^{2}J(Rh–C) is rather unusual but can be justified on the grounds that the coupled nuclei are *trans* about the central rhodium atom.

Further confirmation of these assignments comes from ^{13}C–{^{31}P,^{1}H} measurements which show that both the resonances at 183.1 and 181.7 ppm collapse to simple doublets on irradiation at the phosphorus frequency.

LL = dppe (X).

In the case of the dppe derivative (X) (Table 5), the ^{31}P and ^{13}C NMR spectra are similar to those of (IX) except for the absence of the fine structure arising from ^{31}P–^{31}P coupling through the CH_2 bridge of dppm in (IX). Consequently the NMR spectra of (X) are simpler than those of (IX) and can be, interpreted (Table 5) on the basis of the stereochemical discrimination of the couplings described above for analogous phosphine substituted derivatives. Two types of the ^{31}P–^{13}C couplings are observed in the ^{13}C spectrum: ^2J(P–C) (ca. 10 Hz) for the carbonyl group C(6)O coordinated to Rh(B) and ^3J(P–C) (ca. 20 Hz) for C(7)O and C(9)O which are both in the *trans–trans* positions (**P4**) with respect to the phosphorus atoms of dppe. The ^{31}P spectrum of (X) consists of a simple doublet due to the chemically equivalent phosphorus atoms of dppe and the absence of P–P′ coupling.

3. Conclusions

Solution NMR data show that the solid state structures of the mono- and di-substituted derivatives of $Rh_6(CO)_{16}$ are retained in solution. Important additional information for the assignment of the carbonyl resonances can be obtained from ^{13}C–{^{103}Rh} measurements and, for clusters containing phosphorus donor ligands, from a consideration of long range P–C couplings which provide complementary results. Detailed analysis of 2- and 3-bond ^{31}P–^{13}C couplings, in the P–Rh–Rh–C fragment has been carried out. ^{3}J(P–CO) is more dependent on the inter bond angle(s) than the dihedral angle *viz* ^{3}J(P–C) reaches a maximum for a *trans–trans*-configuration and is not observed for the *cis–cis*, *cis–trans* or *trans–cis* configurations. Furthermore, ^{3}J(P–C) for

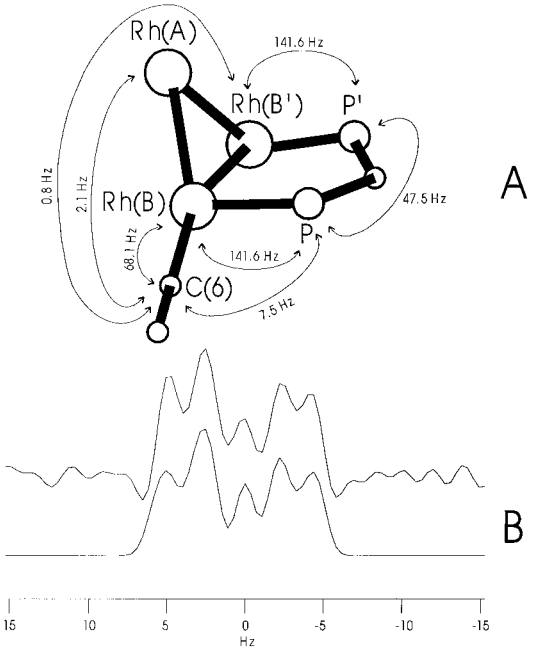

Fig. 14. (A) Schematic representation of the coupling network used in the simulation of the resonance centered at 184.44 ppm (assigned to C(6)) in the ^{13}C NMR spectrum of $Rh_6(CO)_{14}$(dppm). The values of the coupling constants are indicated by arrows. (B) Top: experimental (125 MHz, SW = 24 kHz, TD = 32 K, SI = 128 K, Lorentz to Gauss resolution enhancement with LB = −5, GB = 0.5) and bottom: simulated low field component of the doublet of multiplets.

the *trans–trans* configuration is larger than $^2J(P-C)$ for a *cis*-arrangement. These self-consistent correlations provide a useful starting point for the interpretation of the NMR spectra of other substituted clusters and further studies are underway to confirm the generality of these results.

The observed variable temperature spectra of $Rh_6(CO)_{15}(PPh_3)$ can be explained by a simple oscillation of the PPh_3 on the substituted Rh aided by concomitant exchange of the unique terminal CO on this Rh with the adjacent μ_3-CO's.

4. Experimental

All compounds used in the present study were synthesised according to published procedures: $Rh_6(CO)_{15}L$, L = NCMe [24], py [10], cyclooctene [12], PPh_3 [10], (μ_2-η^1:η^1-dppe) [18], $P(OPh)_3$ [19]; $Rh_6(CO)_{14}(LL)$, (LL = dimethylbutadiene [17], dppe [18], dppm [25], $(P(OPh)_3)_2$ [22]). The ^{13}C and ^{31}P NMR spectra were recorded on a Bruker AM500 spectrometer and $^{13}C-\{^{103}Rh\}$, $^{13}C-\{^{31}P\}$ and $^{31}P-\{^{103}Rh\}$ NMR measurements were carried out as described previously on Bruker WM200 WB and WM250 spectrometers [6].

Acknowledgements

This work was supported by INTAS-RFBR grant No. 95-IN-RU-242 and by an ORS award (to JS). We thank also Dr. V.A. Gindin of the Research Institute of Antibiotics and Medical Enzymes, St. Petersburg, Russia, for permission to use the Bruker AC-200 instrument and Johnson-Matthey Ltd. for the generous loan of rhodium chloride.

References

[1] A. Fumagalli, T.F. Koetzle, F. Takusagawa, P. Chini, S. Martiningo, B.T. Heaton, J. Amer. Chem. Soc. 102 (1980) 1740.
[2] B.T. Heaton, L. Strona, R.D. Pergola, L. Garlaschelli, U. Sartorelli, I.H. Sadler, J. Chem. Soc., Dalton Trans. (1983) 173.
[3] C. Allevi, M. Golding, B.T. Heaton, C.A. Ghilardi, S. Midollini, A. Orlandini, J. Organomet. Chem. 326 (1987) C19.
[4] S. Bordoni, B.T. Heaton, C. Seregni, L. Strona, R.J. Goodfellow, M.B. Hursthouse, M. Thornton-Pett, S. Martinengo, J. Chem. Soc., Dalton Trans. (1988) 2103.
[5] M. Bojczuk, B.T. Heaton, S. Johnson, C.A. Ghilardi, A. Orlandini, J. Organomet. Chem. 341 (1988) 473.
[6] C. Allevi, S. Bordoni, C.P. Clavering, B.T. Heaton, J.A. Iggo, C. Seregni, L. Garlaschelli, Organometallics 8 (1989) 385.
[7] D.T. Brown, T. Eguchi, B.T. Heaton, J.A. Iggo, R. Whyman, J. Chem. Soc., Dalton Trans. (1991) 677.
[8] B.T. Heaton, L. Strona, S. Martinengo, D. Strumolo, R.J. Goodfellow, I.H. Sadler, J. Chem. Soc., Dalton Trans. (1982) 1499.
[9] P. Chini, S. Martinengo, G. Giordano, Gazz. Chim. Ital. 102 (1972) 330.
[10] S.P. Tunik, A.V. Vlasov, A.B. Nikol'skii, V.V. Kryvikh, M.I. Rybinskaya, Metallorg. Khim. 3 (1990) 387.
[11] S.P. Tunik, S.I. Pomogailo, G. Dzhardimalieva, A.D. Pomogailo, I.I. Chuev, S.M. Aldoshin, A.B. Nikol'skii, Izvesiya Akademii Nauk, Serija Khim. 5 (1993) 975.
[12] S.P. Tunik, A.V. Vlasov, A.B. Nikol'skii, V.V. Kryvikh, M.I. Rybinskaya, Metallorg. Khim. 4 (1991) 586.
[13] S. Rossi, K. Kallinen, J. Pursiainen, T.T. Pakkanen, T.A. Pakkanen, J. Organomet. Chem. 419 (1991) 219.
[14] A.L. Rheingold, C.B. White, P.D. Macklin, G.L. Geoffroy, Acta Crystallogr., Section C 49 (1993) 80.
[15] V.G. Albano, P.L. Bellon, M. Sansoni, J. Chem. Soc., A (1971) 678.
[16] G. Ciani, A. Sironi, P. Chini, S. Martinengo, J. Organomet. Chem. 213 (1981) C37; P. Chini, S. Martinengo, G. Garlaschelli, J. Chem. Soc., Chem. Commun. (1972) 709.
[17] Z. Hou, Y. Wakatsuki, H. Yamazaki, J. Organomet. Chem. 399 (1990) 103.
[18] S.P. Tunik, A.V. Vlasov, N.I. Gorshkov, G.L. Starova, A.B. Nikol'skii, M.I. Rybinskaya, A.S. Batsanov, Yu.T. Struchkov, J. Organomet. Chem. 433 (1992) 189.
[19] D.H. Farrar, S.P. Tunik, unpublished data.
[20] J. Mason (Ed.), Multinuclear NMR, Ch. 4 and 13, Plenum Press, New York, 1987.
[21] M. Karplus, J. Chem. Phys. 30 (1959) 11.
[22] S.P. Tunik, A.V. Vlasov, K.V. Kogdov, G.L. Starova, A.B. Nikol'skii, O.S. Manole, Yu.T. Struchkov, J. Organomet. Chem. 479 (1994) 59.
[23] PANIC, Spectral Simulation Program, Bruker Spectrospin, Coventry, 1985.
[24] S.P. Tunik, A.V. Vlasov, V.V. Kryvikh, Inorg. Synth. 31 (1996) 239.
[25] D.F. Foster, B.S. Nicholls, A.K. Smith, J. Organomet. Chem. 236 (1982) 395.